



The relationship between the cutting-edge, tool wear, and chip formation during Inconel 718 dry cutting

Cristian Pérez-Salinas^{1,3} · L. Norberto López de Lacalle² · Ander del Olmo³ · Ch Sateesh Kumar³

Received: 24 March 2024 / Accepted: 23 April 2024
© The Author(s) 2024

Abstract

This study comprehensively addresses the machining of nickel alloys, focusing its attention on crucial aspects related to chip formation and tool wear. Detailed characterization of the morphology and the chip formation process was performed by analyzing parameters such as chip segmentation ratio and variables such as shear band thickness and strain rate. Additionally, a numerical model was used to quantify stresses and temperatures at the tool/chip interface and to evaluate damage, thus contributing to the understanding of the development of chip formation. A transition in chip shapes as the tooling increases is highlighted, evidenced by segmentation ratio values below 0.5, indicative of the presence of discontinuous chips. The increase in cutting-edge radius is associated with a gradual increase in the compression ratio, indicating a higher plastic energy requirement in chip formation. Numerical simulations support this theory of failure. A significant correlation of 80% was identified between flank wear and the increase in shear force oscillation amplitude, indicating that flank wear contributes to system vibration. It is also noted that the adiabatic shear bands (ASB) are narrow, revealing a marked plastic deformation in the primary shear zone. Consequently, the remarkable incidence of wear with cutting parameters on chip formation is demonstrated, affecting the cutting force amplitude and, hence, the workpiece topography.

Keywords Dry broaching · Inconel 718 · Cutting-edge geometry · Tool wear · Chip morphology · Segmentation ratio parameters

1 Introduction

Inconel 718 distinguishes itself as a nickel superalloy thanks to its remarkable mechanical properties. Its composition, which includes significant amounts of chromium, iron, niobium, and molybdenum, among others, gives this alloy unique characteristics, such as exceptional mechanical strength, creep resistance, and long fatigue life [1, 2]. Inconel 718's ability to preserve its structural integrity, even in extreme temperature conditions (below 650 °C) and corrosive environments, positions it as an invaluable material

in the aerospace industry and other applications that demand strength and durability in demanding environments [3].

Cutting forces and data recording in the broaching of Inconel 718 are current research lines [4–7]. From the 1960s to the present day, Inconel 718 has become an essential material in key industries requiring high-performance components, and demand for it continues to rise steadily thanks to its excellent service properties [1]. However, the complexity associated with machining this material is its main challenge. The reasons for this complexity are diverse and have been extensively studied [2, 8, 9]. They include a marked propensity for built-up edge (*BUE*) formation, work hardening behaviors that generate high cutting forces, rapid tool wear due to hard abrasive carbide particles, strength retention at elevated temperatures, low thermal conductivity resulting in high cutting temperatures, and high hardness. In addition, the magnitude of the influence of these behaviors are intrinsically linked to cutting speed, along with other cutting parameters such as tool geometry and feed rate [10, 11]. Therefore, the chip formation of Inconel will exhibit a particular behavior due to the influence of all the effects

✉ Cristian Pérez-Salinas
cperez072@ikasle.ehu.eus

¹ Faculty of Civil and Mechanical Engineering, Universidad Técnica de Ambato, Ambato, Ecuador

² Department of Mechanical Engineering, ESI Bilbao, University of the Basque Country, Bilbao, Spain

³ Aeronautics Advanced Manufacturing Centre (CAA), University of the Basque Country (UPV/EHU), Bizkaia Technology Park - Ed.202, 480170 Zamudio, Spain

added to the tool wear which is a real phenomenon in the chip removal process.

In the aircraft industry, turbine blades can be named as one of the most challenging parts in the production of aircraft engines, due to their criticality, high surface quality, and tolerance [3]. In turbine discs, one of the latest features to be manufactured are the Firtrees for turbine blade mounting. Due to the demanding service conditions, the turbines are manufactured from Inconel 718 and the Firtrees are machined by broaching [12]. Broaching is the certified process that meets all standards for the manufacture of turbine blade Firtrees [13, 14]. Broaching is a type of intermittent orthogonal cutting using relatively low speeds (< 15 m/min). It uses the tool called broaching which is composed of a progression of multiple cutting edges that at the total passage through the workpiece forms the desired profile. To cope with the resistance of Inconel 718 and to optimize efficiency in the cutting process ($V_c = 15\text{--}35$ m/min), specially designed broaches with tungsten carbide inserts are used [15]. The selection and use of these specialized tools underline the importance of research, and the proper control and management of chip formation under real working conditions during broaching. These considerations are critical to preserving the surface integrity of the components.

A worn tool also has an impact on chip morphology. Numerous studies have focused on understanding the complexities of sawtooth chip formation related to flank wear [8, 16–18]. It was observed that both aspects not only have an impact on the quality of the machined surface, but also on the tool life. That is, the configuration and flow of the chip on the tool surface play a significant role in the wear process. Authors such as Anti et al. [16] supported the hypothesis that variations in the level of tool wear directly affect the chip shape and type of segmentation. This support is based on an analysis of both the chip generated and the vibration signals during machining. In a study by Ozcatalbas [19], chip shape was examined at macroscopic and microscopic levels as a function of different cutting regimes, also considering the degree of tool wear. The results of this work concluded that the emergence of chip segmentation is favored by increases in work material hardness, cutting speed, feed rate, negative angle of attack, and flank wear width. In addition, it was shown that the generation of segmented chips during machining leads to impulse forces, which, in turn, generate vibrations in the tool.

In the Inconel 718 cutting process, the serrated chips form easily with an adiabatic shear band reflecting inhomogeneous plastic deformation [20, 21]. This ease of serration is related to the increase in cutting speed [22]. It has been discovered that jagged chips can influence mechanical and thermal loads and cause fluctuation of cutting force. In works such as Chandra [23] and Cui et al. [24], it was demonstrated by the good agreement of the frequency of tooth chip segmentation and the frequency of cutting force fluctuation for turning and milling operations, respectively. The literature shows that cutting force fluctuation is mostly due to changes in cutting speed and feed rate. Jagged chips and fluctuation of cutting force are estimated to be detrimental to surface integrity [18]. Therefore, understanding the phenomenon is of great importance for machining surface quality.

Despite the abundance of studies that focus on simulations and experiments to understand chip formation during machining of Inconel at speeds above 50 m/min, commonly used in turning and milling operations, there is still little comprehensive research on chip segmentation at low speeds (< 50 m/min), such as those used in processes like broaching, and its relationship with cutting and wear parameters. Therefore, filling this gap becomes relevant, since broaching presents a particular working mechanism compared to other chip removal methods. The purpose of this work is to contribute significantly to improve the understanding of the chip formation mechanism and the type of segmentation under low-speed conditions. In addition, it provides crucial information that could be used in the subsequent development of a tool wear identification and process monitoring system, consolidating as a valuable input for future advances in the optimization of these operations [13, 25].

2 Materials and methods

2.1 Work piece and tool materials

A 100-mm-diameter bar of nickel alloy (Inconel 718) was used as a workpiece. Its required and measured chemical composition is given in Table 1. The nickel alloy presented in this work is a heat-treated material by solid solution and precipitation hardening (aging), important to optimize the mechanical properties (Table 2). This material is supplied in its “Annealed” state to improve its machinability [9, 26].

Grain size significantly influences material properties and small grain size increases tensile strength and fatigue

Table 1 Typical composition (weight %) and hardness of nickel-based high-temperature alloy (Inconel 718)

Ni	Cr	Mo	Nb	Ti	Al	Fe	Detail
52.5	19	3	5.1	0.9	0.5	18	AMS5662P [30]
50.2	21.6	2.7	4.7	1.21	0.45	18.1	EDS measurement

Table 2 Mechanical properties of Inconel 718

Properties	Value	Detail
Tensile strength	1310 MPa	[3]
Yield strength	1110 MPa	[3]
Elastic modulus	206 GPa	[31]
Rockwell C hardness	45–47 HRC	Measured
Density	8221 kg/m ³	[31]

resistance. On the contrary, small grain size reduces creep resistance and crack growth [27]. The appropriate size will depend on service conditions and industrial requirements. A grain size that balances all the mechanical properties mentioned is between 50 and 100 microns. The workpiece provided has a microstructure with a large grain size (60 microns on average) surrounded by small grains of opposite size (Fig. 1). The grain size was measured using the intercept method.

Although Inconel 718 offers several mechanical advantages, it also presents challenges in the machining process. The temperature in conventional machining can reach up to 900 °C (turning and milling); in broaching, because of the relatively low cutting speed, it can reach process temperatures between 400 and 600 °C. However, the stability of nickel in its austenitic form up to its melting point, the low diffusion rate of FCC metals which confers good microstructural stability at very high temperatures, the presence of hard abrasive particles in the microstructure, and the high work hardening rates are the main reasons for the difficulty in machining nickel alloys [9, 28, 29].

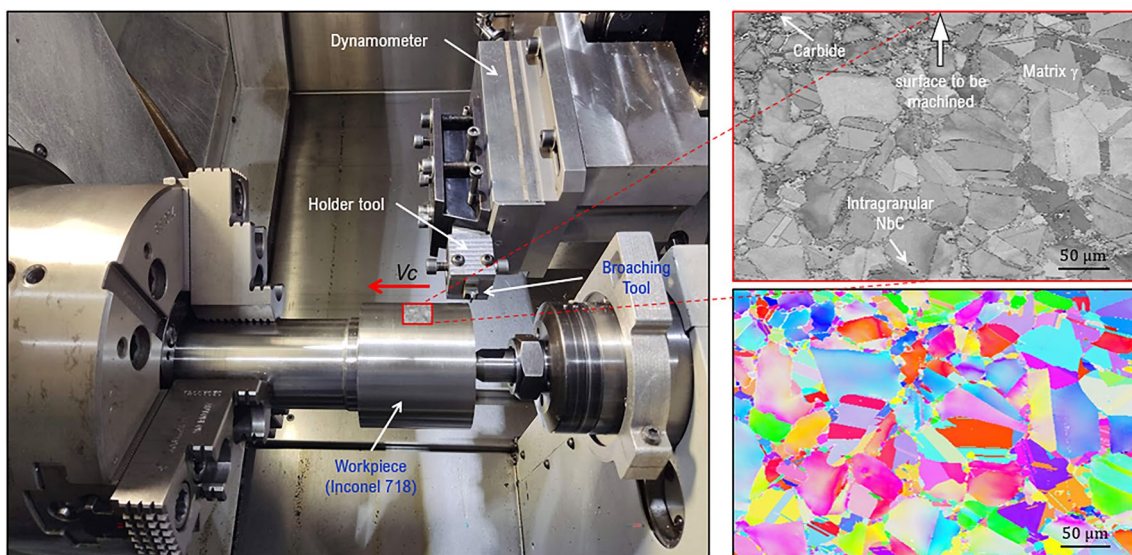
2.2 Experimental setup

The dry cutting experiments were performed on a turning center (CMZ-TC25). The cutting conditions used during these tests are given in Table 3. A Kistler 9129AA dynamometer was used for the shear force measurements. With a Kistler 5011B charge amplifier, the converted signals are recorded at a sampling frequency of 12 kHz. To determine the flank wear of the tool, some images were taken by optical microscopy. SEM microscopy (Tezcan) was employed for morphological analysis of chips, tool flaws, and EDS analysis for material analysis and wear mechanisms.

The cutting tool material is uncoated tungsten carbide (WC-10 wt% Co alloy – ISO Code K20-K40). The rake angle is 7° and the rake angle is 5°. To analyze the samples, some chips were collected and embedded in resin. The samples were polished using 180 to 1200 grit silicon carbide paper, then 1- μ m diamond paste was used for final polishing. Electrolytic etching of the samples was performed with Kroll solution. The average grain size was recorded using the linear mean intersection method. An Alicona™ Infinite

Table 3 Experimental cutting conditions

Para	Hardness	Ni
Cutting speed, V_c	(m/min)	20
Cutting width, B	(mm)	8
Rise per tooth, RPT	(μ m)	25, 50, 75
Radius edge, r_β	(μ m)	5, 15, 25, 35

**Fig. 1** Microstructure of Inconel 718

Focus device (G5 series, vertical resolution > 10 nm) was used for chip characterization and grain size measurements.

2.3 Analysis of chip segmentation and morphology

Nickel alloy chip morphology generally depends on contact tribology, cutting conditions, and thermodynamic loading in the cutting action [21]. From the thermodynamic load intensity, the morphology is influenced by the plastic behavior of the material resulting from the interaction between thermal softening and hardening caused by the work performed in the shear zone [32, 33]. The cutting conditions that mainly affect cutting morphology are cutting speed, feed rate, and tool geometry [34]. However, information on the influence of tool cutting edge micro-geometry on chip morphology is scarce. In addition, recent studies such as that of Haimde, Airao, and Gdula [11, 35, 36] reported influence of wear on chip morphology in traditional machining such as milling and turning, but the results were reported qualitatively. Therefore, a quantitative assessment will significantly contribute to the effect of wear on chip morphology.

The analysis of chip morphology provides insight into the cutting process and provides information on the appropriate conditions to be used for a stable cutting process. There are geometrical parameters for the determination of the parameters affecting the chip segment morphology (Fig. 2). Table 4 shows the equations for analyzing chip segmentation and morphology in the machining environment.

The initial evaluation of the chip morphology is performed by the frequency of segmentation during the cutting process, as described in Eq. 1 [37]. Although this parameter provides a basis, it is not sufficient to explain the local deformation experienced by the chip. The chip compression ratio (CR) according to Eq. 2 quantifies the

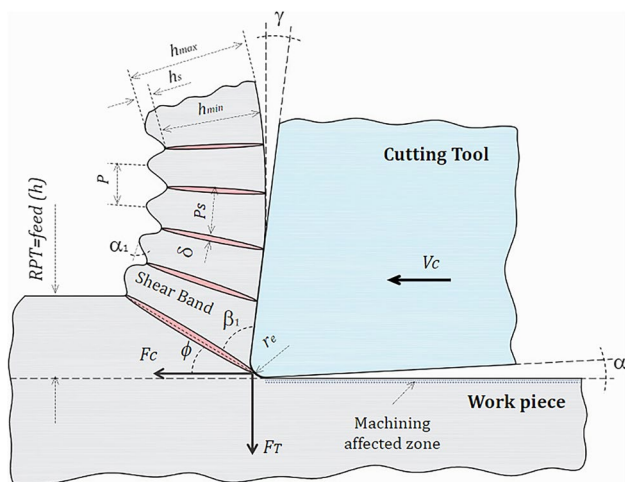


Fig. 2 Segmentation parameters for chip morphology determination

Table 4 Parameters for chip morphology and segmentation determination

Parameter	Equation
Chip segmentation frequency, Hz	$f_{ch} = \frac{100 \cdot v_c \cdot RPT}{6 \cdot P \cdot h_{max}}$ (1)
Chip compression ratio	$CR = \frac{(h_{max} + h_{min})}{2 \cdot RPT}$ (2)
Average chip segmentation ratio	$SR = 2 \cdot \frac{(h_{max} - h_{min})}{(h_{max} + h_{min})}$ (3)
Segmentation Intensity Ratio	$SIR = \frac{\frac{\epsilon_{in}^p}{\epsilon_{out}^p}}{\frac{\epsilon_{in}^p}{\epsilon_{out}^p}} = \frac{mean(\frac{\epsilon_{in}^p}{\epsilon_{out}^p})}{mean(\frac{\epsilon_{max}^p}{\epsilon_{min}^p})}$ (4)
Average strain within the shear band	$\epsilon = \frac{h_s \cdot \sqrt{h_{max}^2 + RPT^2 - 2 \cdot h_{max} \cdot RPT \cdot \sin \gamma}}{h_{max} \cdot \delta \cdot \cos \gamma}$ (5)

plastic deformation of the chip [38]. Higher values of CR indicate a higher plastic energy requirement for chip formation. To better understand the intensity of segmentation, Kouadri et al. [38] introduced the “chip segmentation ratio” (SR) parameter by means of Eq. 3. This parameter quantitatively evaluates the degree of chip segmentation, where 0 corresponds to a continuous chip and 1 to a fragmented chip. If one seeks to quantify the relative variation of the deformation in the chip, Atlati et al. [39] presented the “segmentation intensity ratio” (SIR) parameter based on Eq. 4. Unlike the geometrical parameters, SIR depends on the ratio between the plastic deformations inside and outside the shear-shear bands on the chip, allowing to quantify the relative variation of the deformation at the center of the chip. Thus, chip morphology can be analyzed quantitatively, regardless of the type of chip encountered. The advantage and limitation of SIR lies in its easy determination from finite element modeling under the analyzed conditions, as explained in the method. Finally, by means of Eq. 5, the shear deformation within the shear band under the shear conditions can be observed [40]. This parameter, together with the shear band thickness, provides an idea of the speed and severity of the deformation within the chip at the time of shearing the material [23].

Chip formation has been extensively investigated by several studies in the literature. Chip morphology varies depending on the nature of the workpiece material. In general terms, chips can be classified as continuous, discontinuous, segmented, and catastrophic shear. Segmented chips are further classified as periodic and aperiodic [41]. When machining Inconel 718, it is common to find sawed chips with different levels of intensity. According to Komanduri and Schroeder [20], the initiation and propagation of cracks in the primary shear zone, as well as thermoplastic instability, are responsible for the formation of saw edges in Inconel 718 chips. It has been generally demonstrated that cutting speed is the parameter that most influences the frequency and intensity of chip segmentation. Therefore,

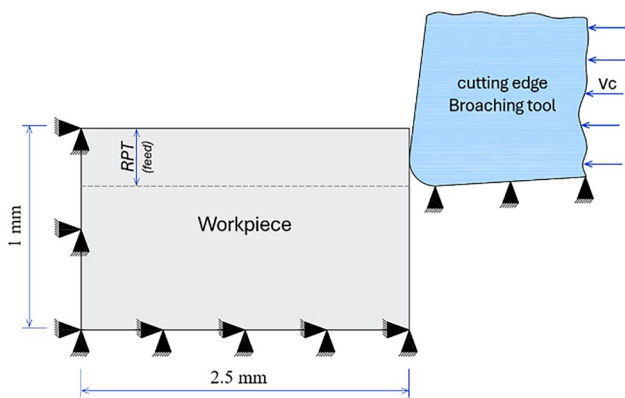


Fig. 3 Finite element modeling geometry and boundary conditions

it is imperative to explore other factors that may influence changes in chip morphology, their impact on shear strength, and their influence on surface quality.

2.4 Chip morphology

The commercial finite element analysis software DEFORM-2D™ was used to simulate the orthogonal cutting process of Inconel 718, where it uses Lagrangian update code with remeshing technique to achieve the mechanical and thermal steady-state conditions during the simulation. The tool was modeled as a rigid body with 8000 elements and the workpiece fully constrained in its six directions (Fig. 3). Initially, the workpiece uses 15,000 isoparametric quadrilateral elements and the software allows refining the element size to 1 μm toward the cutting zone, to obtain more accurate results and better chip geometry. Table 5 shows the equations governing the implemented simulation.

Sawtooth chip formation was simulated using the Johnson-Cook (*JC*) damage model (Eq. 6) [42]. Table 6 presents the set used for this study. The *JC* model describes the plastic deformation of materials in different strains, strain rates, and temperature ranges. This model is useful for modeling material behavior in the simulation of the cutting process where large plastic deformations occur up to strain rates of 1000 s⁻¹ and deformations of about 0.3 during chip formation [43]. In this research, the Cockcroft

and Latham criterion (Eq. 7) was considered to predict the chip segmentation during orthogonal cutting [44].

As for friction modeling, the Coulomb friction model (Eq. 8) is used to represent the frictional interaction at the interface between the tool and the workpiece. A friction coefficient (1.1), experimentally determined under the influence of flank wear [46], was applied for the uncoated carbide cutting tool (WC/Co) during machining of the nickel-based alloy IN718. As pointed out by Arrazola [47], in conventional machining at low cutting speeds, the Coulomb model is effective in describing the friction conditions on the tool flank face.

3 Results and discussion

This section presents the results of the broaching experiments under the conditions determined in Table 1. The morphology of the chips and their parameters obtained under the processing conditions were used to understand the changes in the mechanisms of chip segment formation. This is followed by the presentation of the results on the influence of tool wear and changes of edge radius and *RPT* on the variation of cutting force amplitude and chip morphology.

3.1 Chip morphology

For broaching Inconel 718 machined at a cutting speed of 20 m/min, continuous chips with some levels of serration are generally evident (Fig. 4). In addition, sawtooth chip formation is aperiodic according to the classification given by Davis et al. [41], which is examined on the free surface of the chip. This means that the sawtooth segmentations are interrupted along the width of the chip (Fig. 4). There are three characteristics that allow us to differentiate the morphology of the chips obtained. The first is the level of uniformity of the serrate. The chip profiles shown in the figures illustrate this characteristic, where uniformity depends on the segmentation aperiodicity. This aperiodicity is affected by changes in tool edge radius (Fig. 4a, d, g, and j) and effects caused by increased wear and *RPT* (e.g., Fig. 4d–f). The tendency of the chip to achieve a periodic serration increases with increasing radius and *RPT* with the influence

Table 5 Main equations involved in chip-forming modeling

Model/theory	Equation
The Johnson-Cook plastic deformation model	$\sigma_{yld} = [A + B \cdot \epsilon^n] \cdot \left[1 + \ln\left(\frac{\dot{\epsilon}}{\dot{\epsilon}_0}\right)\right] \cdot \left[1 - \left(\frac{T - T_0}{T_{melt} - T_0}\right)^m\right]$ (6)
Cockcroft and Latham's criterion	$D = \int_0^{\epsilon_f} \sigma_1 d\epsilon$ (7)
Coulomb friction model	$\tau_f = \mu \cdot \sigma_n$ (8)

Table 6 Constants of the Johnson-Cook equation [45]

A (MPa)	B (MPa)	C	n	m	$\dot{\epsilon}_0$	T_r (°C)	T_{melt} (°C)
1485	904	0.015	0.777	1.689	1	20	1300

of flank wear. Wear affects the geometry of the cutting edge, which in turn affects the chip morphology. This phenomenon was observed in other materials such as steel and titanium alloys [16, 48].

The second feature is the presence of primary and secondary segmentation folds (e.g., Fig. 4h and k). These features are influenced by large unstable deformations at the shear edge-material contact at the time of shearing. This instability results in material folds of variable morphology as shown in Fig. 5. According to the report by Davis et al. [41, 49], the researchers deduce that these thin lamellae form because the cutting-edge advances as the microstructure undergoes uniform deformation. Consequently, the microstructure influences the morphology of these lamellae. Finally, the third characteristic is the variability in chip thickness. This change in chip thickness is influenced by cutting conditions. In this study, it is affected by parameters such as cutting-edge geometry and changes in *RPT*, further influenced by vibrations in the system such as the characteristic vibration of the tool clamping system (Fig. 4a, b, and k) and possibly fueled by increased tool wear. An examination of the free surface of the chip in Fig. 4c reveals the type of laminar structure distributed across the width of the chip. As will be demonstrated later, Fig. 4c is evidence of the tendency for the change from a continuous chip to a segmented chip influenced by flank wear.

During the process of continuous chip formation, shear band growth is relatively stable, so all shear bands evolve at the same level (Fig. 4d). However, when moving to the transition of jagged chips, the growth of shear bands is unstable (Fig. 4i). This means that as the deformation evolves, some bands grow faster suppressing others causing instability in the chip thickness. So, the instability of the chip thickness can be seen by different levels of serrate (Fig. 3h) and periodic bands with accumulation at different frequencies (Fig. 4k).

According to the literature, machining of nickel alloys, such as Inconel 718, produces serrated chips due to their high strength and strain hardening. Figure 3 shows non-uniform chip serration, resulting from uneven deformation at each cutting condition. According to the work of Komanduri [32], inhomogeneous deformation is attributed to the high strength of the material, its face-centered crystalline structure, the presence of large grains, and the intense deformation in a narrow region. To Inconel, the appearance of segmented chips is observed at speeds above 30 m/min, while continuous chips are generated at lower speeds [20].

In this study, the broaching feed rate was found to influence the uniformity of the sawing, while the cutting speed was kept constant. At a cutting speed of 20 m/min, continuous chips were produced with non-uniform sawing due to grain size diversity (Fig. 1), intense plastic deformation, and localized heating due to the low conductivity of Inconel [21]. Adiabatic shear instability occurs when local temperature and strain conditions reach a critical point, generating narrow shear bands. This phenomenon is observed in Fig. 6 where the shear bands are thinner than 3 μm . In addition, tool wear and system stiffness could also have affected the sawing intensity and chip morphology, which is reflected in disturbances in the machined surface and amplitude in the cutting force signals as will be shown below [50, 51].

3.2 Chip segment formation mechanism

Chip formation mechanisms are defined through morphological parameters as illustrated in Fig. 2. Figure 5 illustrates in three-dimensional form a continuous chip with periodic serrate and its main characteristics. For all experimental conditions, the chip type was close to the continuous type with a certain degree of serration as detailed in Fig. 6. The total length of deformation that a material undergoes while forming a segment is composed of two sections (blue line). The first section corresponds to the fracture, where the material was completely sectioned and split between two consecutive segments and the second section corresponds to the joined part of two segments where the shear band is located and where the largest plastic deformation is concentrated. The shear band has small thicknesses compared to other heat-resistant alloys such as titanium or hard steels. At a wide range of shear rates, shear band thicknesses (*ASB*) in Inconel are reported to range from 2 to 60 μm [52]. In the present work, thicknesses between 1.5 and 2.75 μm were measured.

The literature summarizes the debate on the formation of jagged chips in two theories, (i) the adiabatic shear theory and (ii) the periodic crack theory [52]. For the present study, the chip formation mechanism is estimated to be more in agreement with theory (i) because a shearing occurs once the critical deformation is overcome. Due to the low thermal conductivity of Inconel 718, the heat generated by plastic deformation often accumulates in the narrow bands located by shear (Fig. 5).

In Fig. 6, it is evident that the segments are bonded over a large part of the length of the shear plane. This implies

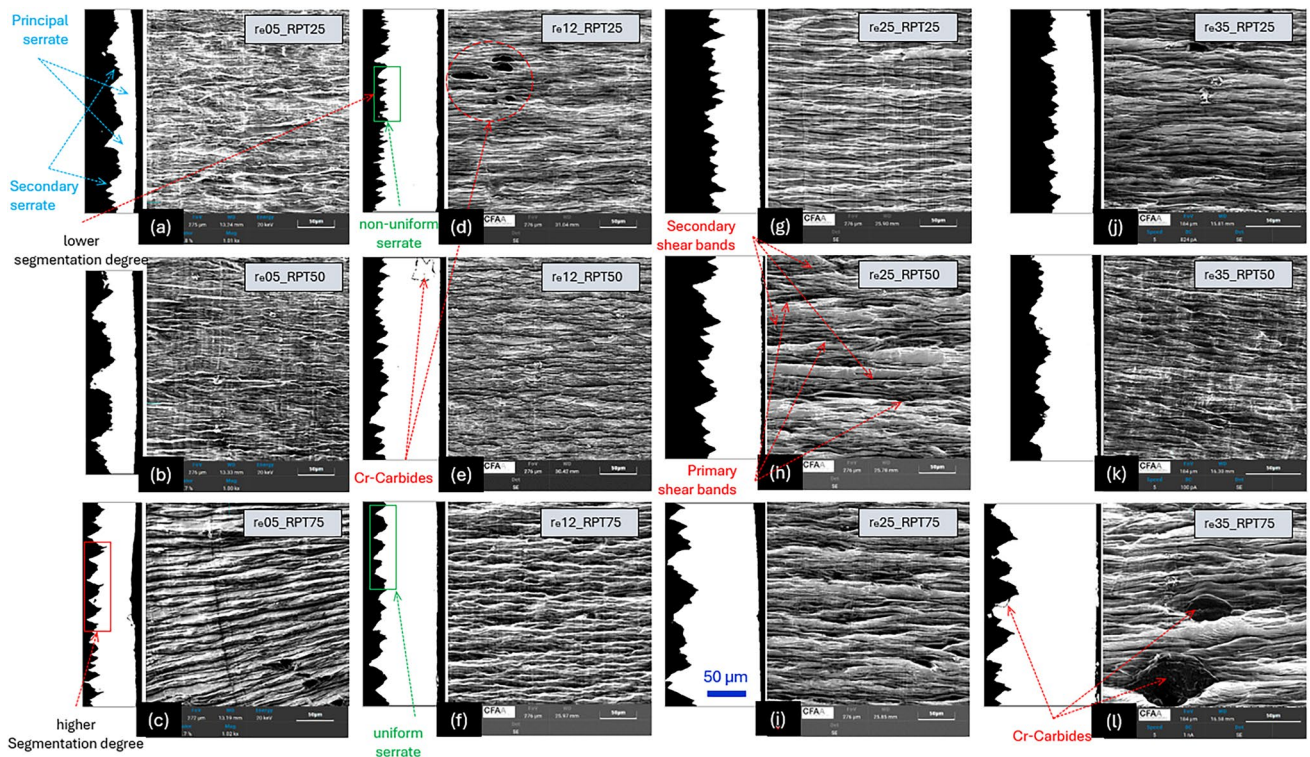


Fig. 4 a–l Cross section and free surfaces of the segmented chips obtained in the machining of aged nickel Inconel 718 alloy at cutting speed of 20 m/min and at the different conditions shown

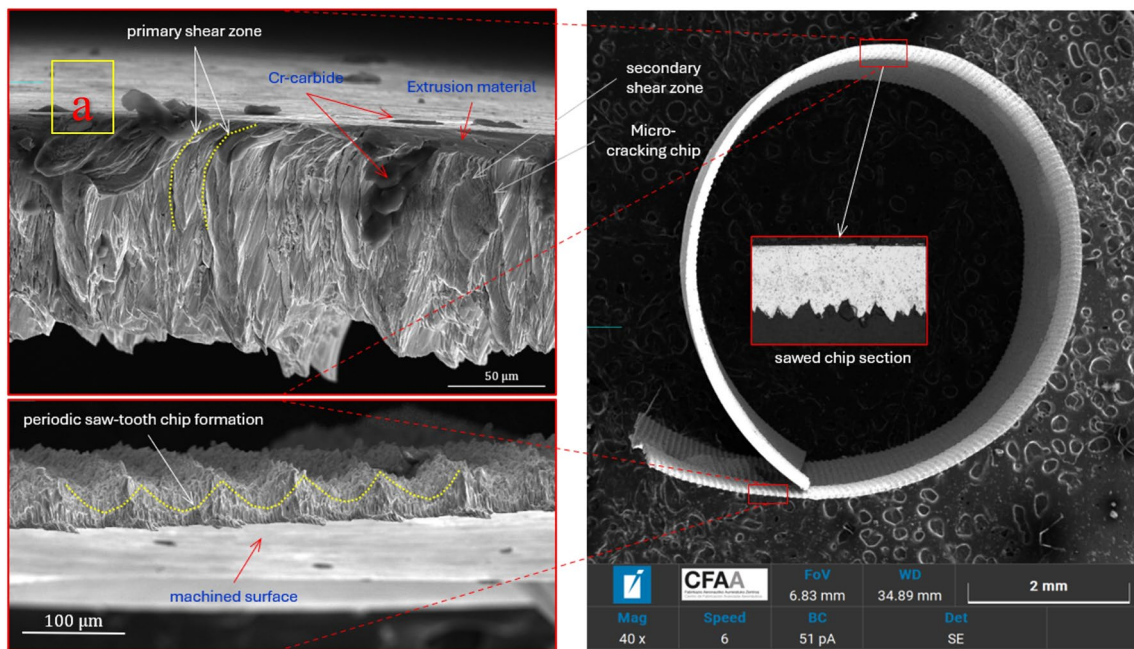


Fig. 5 Periodic sawtooth chip morphology of aged and forged Inconel 718 machined at $v_c=20$ m/min, $r_b=35$ μ m, and $RPT=75$ μ m

that the contribution of plastic deformation is very high in the formation of the chip segment. Explained by Pawade and Chandra [23, 53], two reasons can explain this effect.

Firstly, the machining of Inconel is influenced by shear instabilities, resulting in intense localized deformation in the primary deformation zone. Secondly, the intensity of

Fig. 6 Microstructure of the chip showing the segment formation mechanism

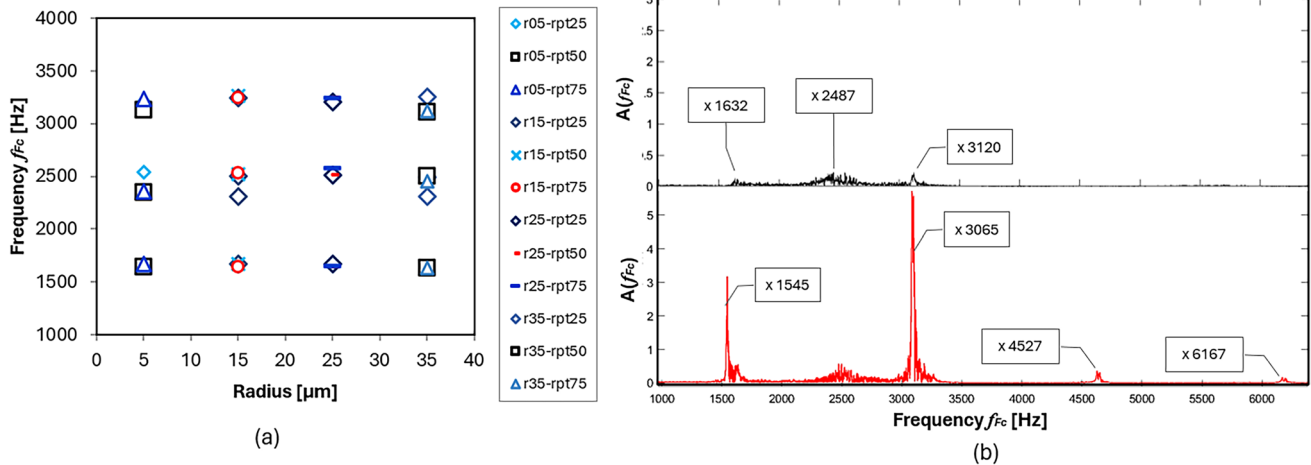
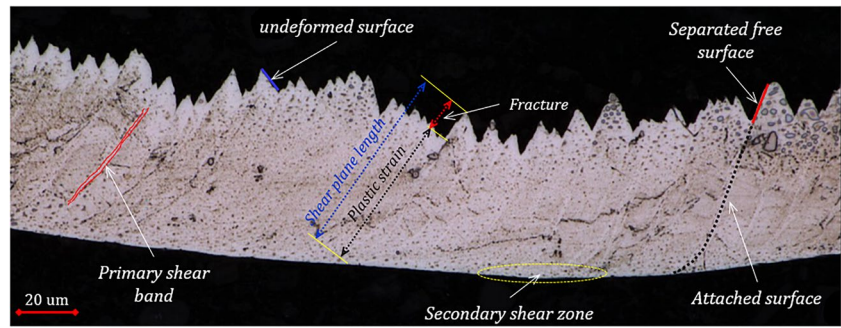


Fig. 7 Behavior of the shear frequency signal when broaching Inconel 718 aged at $v_c = 20$ m/min, **a**) fluctuations at changing cutting-edge radius, **b**) dominant frequencies below flank wear $V_B=0.15\text{ mm}$ (black) and above $V_B=0.15\text{ mm}$ (red)

this localized deformation is attributed to strain hardening, which is a characteristic of machining at low cutting speeds. In addition, evidence of a small fracture section makes the chip distinct from a continuous type chip. It is understood that, during the formation of such segments, the segment being formed slips over the segment below through a slip that is very small. In this type of segment formation, a large part of the cutting energy is consumed in the plastic deformation to fracture the segment [54].

3.3 Analysis of chip segmentation or morphology under different machining conditions

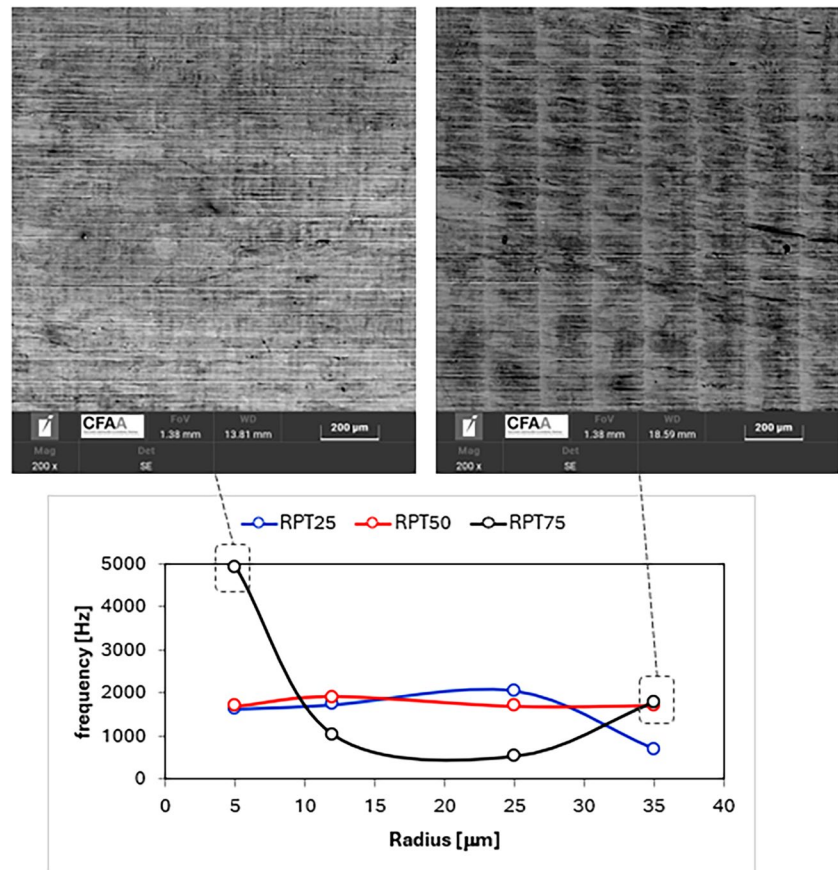
The characteristic frequencies of the shear process (f_{Fc}) were evaluated from the real-time force signal. These were found with flank wear less than 0.15 mm. Figure 7a shows the in-contrast dominant frequencies for all experimental shear conditions. These dominant frequencies are manifested with different amplitude in the range of 1700 to 3500 Hz, with the highest peaks around 1700, 2500, and 3300 Hz, respectively (Fig. 7b). As these frequencies were repeated in all tested conditions, it is presumed that this is due to the characteristic

frequency of the tool clamping system. When the wear was greater than 0.15 mm, other dominant frequencies were found in the frequency spectrum. The highest peaks were 1500 and 3000 Hz and other peaks were 4500 and 6000 Hz, respectively.

On the other hand, the frequency of occurrence of periodic fluctuation on the machined surface (f_{sup}) with V_B tool wear between 0.15 and 0.35 is shown in Fig. 8. From Fig. 8, a wide variation of fluctuation frequency is denoted when working at a RPT 75 μm and where the tool wear is higher. On the other hand, when working at a RPT of 25 and 50 μm , respectively, there is no major variation of f_{sup} . It is identified that the dominant frequency of 1500 Hz of the force f_{Fc} coincides with most of the fluctuation frequencies of the surface f_{sup} . Therefore, it is estimated that it is the dominant frequency of the clamping system or the cause of the damping effect.

The evaluation of the segmentation length (P) and chip segmentation frequency (f_{chip}) parameters is shown in Fig. 9a and b respectively. The chip segmentation frequency was calculated using the geometric shape of the chip (Eq. 1). First, P and f_{chip} show opposite trends; i.e., if P is reduced,

Fig. 8 Frequencies of topographic fluctuation in the mechanized surface



the frequency increases and its corresponding inverse effect. On the other hand, the segmentation frequency tends to decrease with increasing cutting-edge radius of the tool, while the chip segmentation length decreases. This effect is a characteristic for radii greater than 15 μm and the effect is the opposite for radii greater than 15 μm . This behavior is replicated to a greater or lesser degree for each *RPT* with the most noticeable growth for *RPT* = 50 μm . At a general level, f_{chip} and P give an indication of the number of shear bands within the same chip length and are the first basic indicators of analysis.

As shown in Fig. 8c, the chip reduction coefficient (*CR*) values tend to increase with increasing cutting-edge radius (r_β). As mentioned by Biskash et al. [23], higher values of the *CR* property indicate a higher plastic energy requirement for chip formation. Consequently, a larger cutting-edge radius will require more plastic energy for chip formation. On average, 50% more energy is used for a 5- μm edge radius than for a 35- μm cutting edge radius. On the other hand, Fig. 8d shows the results of chip segmentation ratio (*SR*). An average decrease in the surface roughness ratio (*SR*) of 55% is observed when varying from the smallest to the largest cutting-edge radius for all milling tools (*RPT*). This translates into a reduction of the average *SR* value from 0.81 to 0.39, respectively. Since *SR* represents the level of serration

on a scale from 0 to 1, where 1 indicates a continuous chip, the increase in cutting edge radius causes an increase in serration. Furthermore, it should be noted that most of the chips obtained (Fig. 4) have *SR* values in the range of 0.20 to 0.48. This indicates that all chips are in the transition from a continuous chip to a segmented chip.

The behavior of the adiabatic shear band width (*ASB*) and the variation of shear band deformation with the change of shear edge radius are shown in Fig. 10a and b, respectively. According to the trend obtained from Fig. 10a, it can be found that the width of the band increases with the increase of cutting-edge radius (r_β). A growth of the shear band from 50 to 70% of the thickness because of r_β is evident. The trend is maintained in the face of the change in *RPT*. This increasing trend of the shear band may be due to lower concentrated strain rate produced by thermal softening [55], and this same behavior can be seen in Fig. 10b. The heat produced by the plastic flow within the shear band has a shorter time to transfer to the environment by diffusion, resulting in a widening of the heat-affected zone.

The literature indicates that the shear bandwidth in nickel alloys exhibits sensitivity to variations in shear rate (see Table 7). Unlike other materials, the bandwidth in nickel alloys is narrower, especially when compared to titanium alloys and hardened steels. Even at extremely high

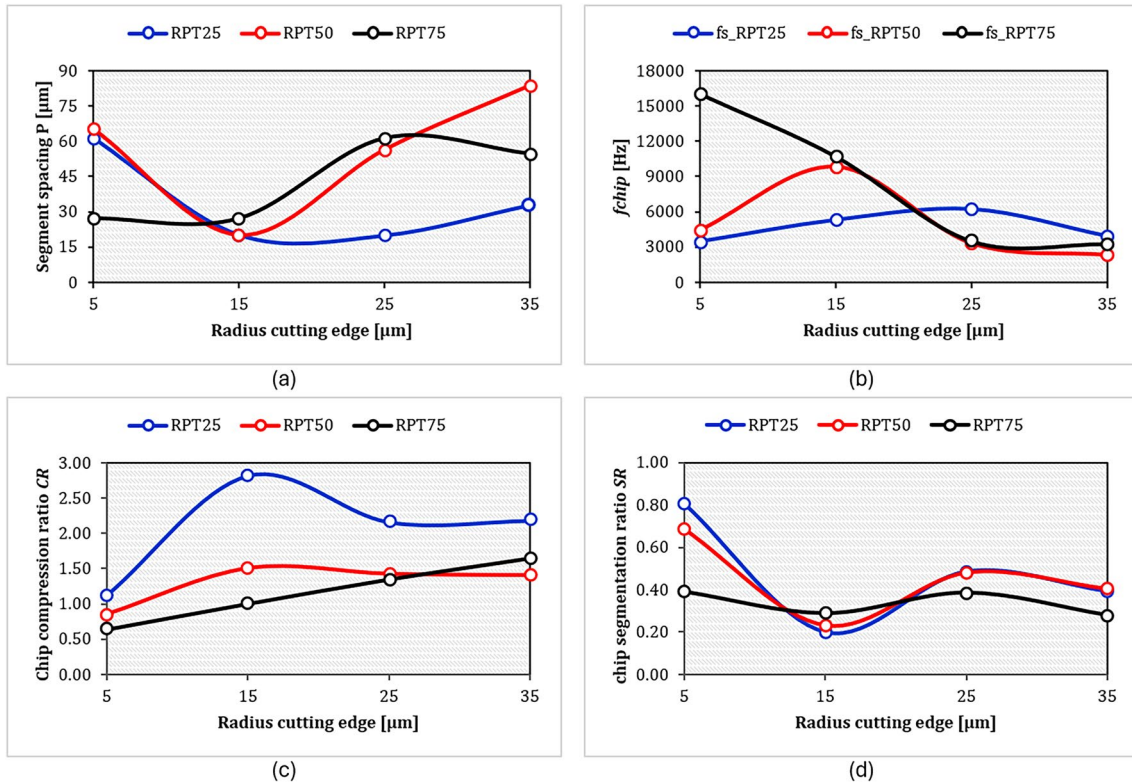


Fig. 9 Elementary chip morphology and segmentation analysis parameters: **a** segment spacing P , **b** chip frequency f_{ch} , **c** chip compression ratio (CR), and **d** chip segmentation ratio (SR). Broaching of Inconel 718 at $v_c = 20$ m/min

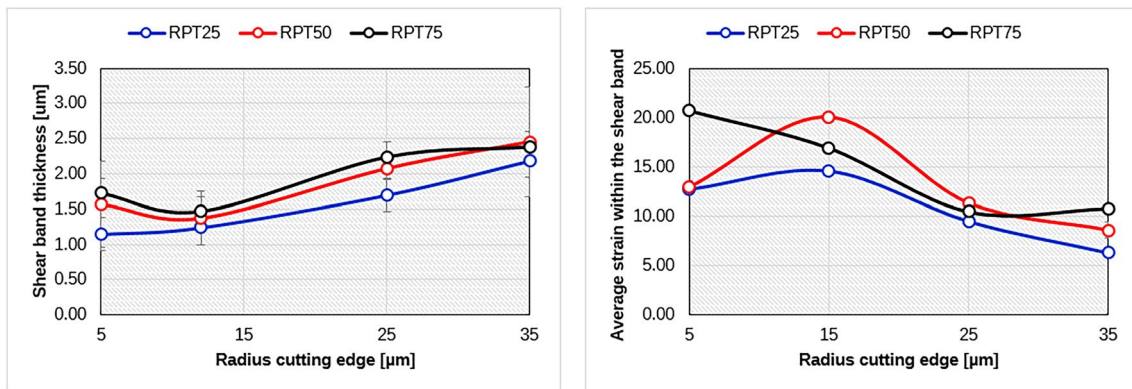


Fig. 10 Analysis of the shear band under edge radius changes at different rise per tooth (RPT). **a** Shear band thickness and **b** deformation variation in the shear band. Broaching of Inconel 718 aged at $v_c = 20$ m/min

deformation conditions, such as those evaluated by the Split-Hopkinson pressure bar test, the variation in chip thickness remains in the range of 2 to 4 μm , as reported by Clos [56]. However, the emergence and development of ASB is not limited exclusively to shear rate; it is a complex phenomenon influenced by several variables, including shear edge geometry, material properties, strain rate, temperature dependence of the flow stress, strain hardening rate, and thermal conductivity, among others [52]. Therefore, in the context of this

study, it can be summarized that the width of the shear band can be attributed to the effects of the temperature increase within the shear band and the growth of the cutting-edge radius.

3.4 Analysis of single-segment chip generation

Figure 11 shows the damage evolution of Inconel 718 during the generation of a chip segment, which was

Table 7 Variation of the width of the band *ASB* with changing cutting speed

vc (m/min)	Temp (°C)	<i>B</i> (mm)	Feed (mm)	ASB (μm)	Cutting process	Reference
40	T_{room}	1	0.2	95	Orthogonal turning	[23]
80	T_{room}	1	0.2	16	Orthogonal turning	
120	T_{room}	1	0.2	13	Orthogonal turning	
80	T_{room}	-	-	19	Orthogonal turning	[57]
100	T_{room}	-	-	17	Orthogonal turning	
140	T_{room}	-	-	14	Orthogonal turning	
50	T_{room}	1	-	6	Pendulum-based cutting test	[55]
140	T_{room}	1	-	2.5	Pendulum-based cutting test	
100	30	1.5	0.13	9	Orthogonal turning	[34]
100	300	1.5	0.13	7	Orthogonal turning	
100	600	1.5	0.13	3	Orthogonal turning	

obtained by simulation using 2D Deform. The simulation process was carried out following the procedure described in a previous work [46]. The Cockcroft-Latham damage model used by Deform has proven to be a good indicator of material degradation for cutting processes. According to the simulation, the chip deformation process occurs over a period of 870 ms. Steps 1–4 show the development of the shear band from the tool tip to the free chip surface with the tool feed. The displacement of the shear band is shown in steps 5–8, at this stage you can see the further displacement of the material with a tendency to form the chip curvature. Stage I, a decrease in shear force should be observed due to a loss in material stiffness propagating through the shear band, while the feed force increases as the opposite effect. Stage II, the shear force recovers because of the transfer of the damaged material and, conversely, a reduction of the feed force is found, which can be supported by the evolution of the shear force and the feed force.

The *SIR* parameter is defined as a ratio between the equivalent plastic strain inside and outside the adiabatic shear band between successive bands. The *SIR* was determined by employing Eq. 4 and from the equivalent deformation results provided by *FEM* analysis (Fig. 12a). From Fig. 12b, it can be distinguished that there are no significant changes in the chip segmentation intensity in the three *RPT* domains. For a *RPT* = 25 μm, the *SIR* experiences a slight increase when the cutting-edge radius grows. However, for the other *RPT* values, there is no clear trend. Previous studies such as that of Kouadri [38] and Yaich [58] showed that the chip segmentation index (*SIR*) exhibits greater sensitivity to variations in cutting speed and rake angle in other ductile aircraft materials, such as aluminum and titanium alloys, respectively. Furthermore, they have shown that at relatively low speeds no substantial change in *SIR* is observed, which supports the results obtained in this study. Therefore, working with a constant low speed in the

investigated cutting radius ranges does not significantly influence chip formation in Inconel 718.

Atlati et al. [39] demonstrated the presence of a correlation between chip segmentation intensity and average cutting force. It was observed that, as the cutting speed increases, the average cutting force decreases, and the chip segmentation index (*SIR*) increases. In contrast, in the cases analyzed in this study, where machining was carried out at a constant speed, the influence of the cutting-edge radius on the cutting force was highlighted. In other words, as the segmentation intensity increases, a decrease in cutting force is recorded (Fig. 13).

3.5 Influence of tool wear

Based on the results of the degree of *SR* chip segmentation and tool wear, a diagram showing the correlation between these two variables is shown in Fig. 14. The points shown in the figure correspond to the wear at the end of the test under the corresponding conditions. Figure 14 shows that during the initial phase (tool with small flank wear), a continuous chip is generated. Once a certain degree of tool wear is reached, the chip changes its forming mechanism, resulting in a sawtooth chip shape. This change in geometry and cross-sectional shape is gradual and without abrupt transitions from one shape to another. Certain variations in the degree of chip deformation observed during the experiment can be attributed to accumulations on the cutting-edge, i.e., to the change in cutting geometry during the cutting process. Thus, at lower cutting speeds, both tool wear and built-up edge (*BUE*) are two sources of alteration in cutting-edge geometry, which impacts chip formation and morphology. This influence of wear on the change of chip morphology is a recurring phenomenon in other difficult machining materials, such as titanium alloys [48, 59], while *BUE* is a characteristic in machining Inconel [60] and other materials at low cutting speeds [61].

Fig. 11 **a** BUE formation at the cutting edge, **b** Distribution of material degradation during the generation of a chip segment

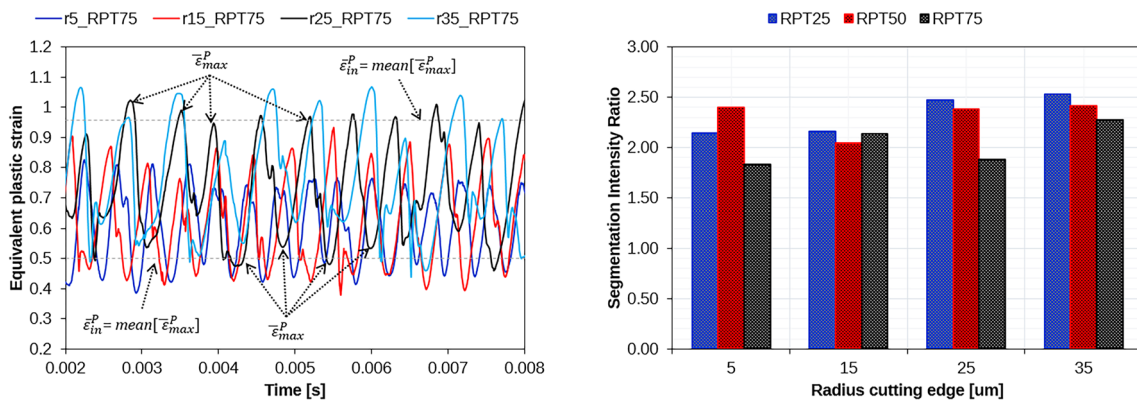
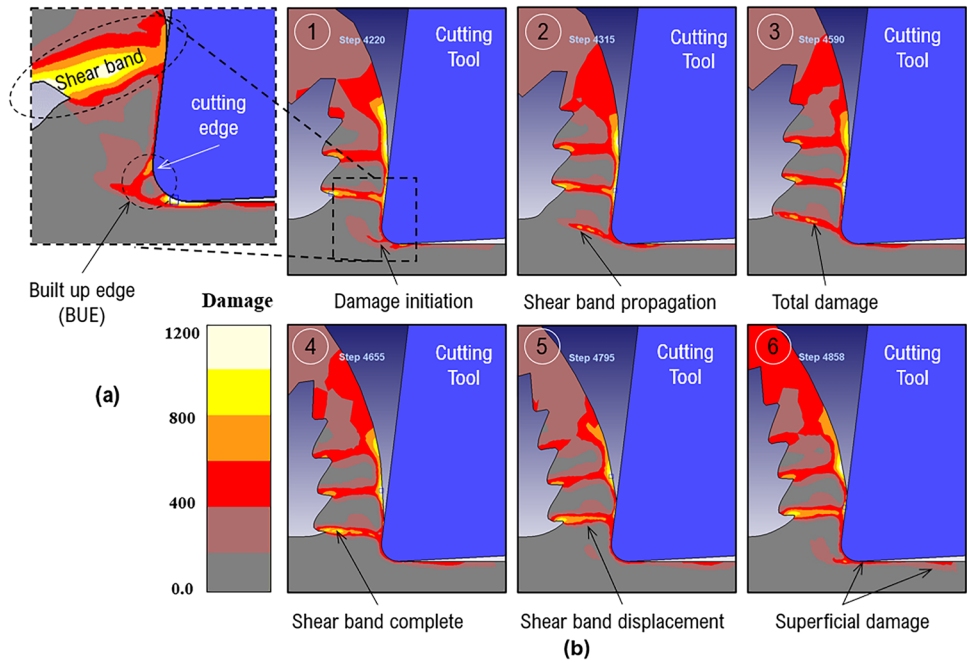


Fig. 12 Equivalent localized plastic strain in the middle zone of the chip. **a** Obtained by FEM analysis for shear edge radii 5, 15, 25, and 35 μm at a RPT = 75 μm and $v_c = 20$ m/min. **b** SIR segmentation intensity ratio for all shear conditions

One of the key parameters defining the character of vibrations during machining is the chip generation frequency of the blades. Figure 15 illustrates the change of chip generation frequency due to varying flank wear depth. The chip generation frequency decreases with the progression of the flank wear depth. This decrease is especially noticeable when switching from a 25-μm RPT to a 50-μm RPT, achieving an approximately 50% reduction in F_{ch} . Subsequently, the decrease in F_{ch} is more moderate. Consequently, the increase in feed rate per tooth (RPT) and wear results in a reduction in chip generation frequency. Anti et al. [16] reported on the impact of wear on frequency variation for different depths of cut, noting that maintaining a wide frequency range can cause significant fluctuations in cutting force at the cutting-edge of the tool.

Figure 16 presents the evolution of the amplitude of the resultant cutting force (A_{Fc}) as a function of the variation of the cutting-edge radii (r_{β}). An increase in A_{Fc} is observed from a radius of 5 to 15 μm, remaining high for a radius of 25 μm and then decreasing for a radius of 35 μm. This behavior is hardly noticeable for a 25-μm RPT, but noticeable for 50- and 75-μm RPT, respectively. The growth trend of A_{Fc} is consistent for the 5 and 15 radius cases but differs for the 25-μm and 35-μm radii cases. There is a significant increase in amplitude from RPT 25 μm to RPT 50 μm, balancing out for RPT 75 μm. When relating A_{Fc} to V_B flank wear, a correlation coefficient close to 80% was found, indicating that the increase in flank wear influences the growth of A_{Fc} in all the cases studied. It is suggested that flank wear induces vibrations in the system, contributing to the increase of A_{Fc} . Previous research supports this idea,

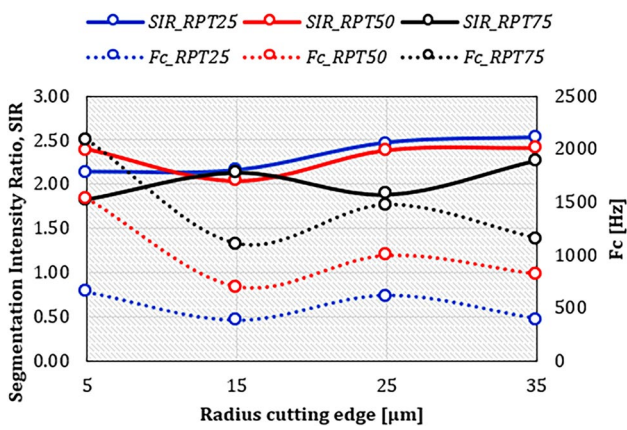


Fig. 13 Correlation between average cutting force and broached segmentation intensity ratio a and $v_c = 20$ m/min at different cutting-edge radii and RPT

showing changes in cutting signals due to tool wear, attributed to higher energy release during discontinuous chip formation and increased friction at the chip/tool interface [13, 16, 62]. In this study, increased force amplitude is largely attributed to increased flank wear, as illustrated in Fig. 16.

Several previous studies reported that force amplitude has a directly proportional increasing relationship with cutting speed in various conventional machining operations at low, high, and very high levels [23, 24, 50]. It was concluded that the increase in the degree of chip toothing caused a significant change in cutting thickness during sawtooth formation, resulting in a

greater amplitude of cutting force. In addition, investigations such as those carried out by Sun [51] and Belhadi [50] reported an increase in A_{Fc} with increasing feed rate for titanium alloy and AISI 4340 steel, respectively. This behavior is attributed to the combined effect of the low modulus of elasticity and the change in material cross section. In the context of this study, it is observed that the effect of cutting speed is null, since it remained constant during the machining process. However, variations were made in the cutting-edge radius and RPT . Based on the results obtained, a contour plot was constructed to visualize the combined effect of these parameters on the cutting force amplitude and its relationship with tool wear (Fig. 17).

Figure 17a reveals that the shear force amplitude (A_{Fc}) is practically constant for all cutting-edge radius (r_β) when the values of flank wear (V_B) are less than 0.12 mm. However, from values higher than $V_B = 0.12$ mm, the amplitude tends to decrease as r_β increases. On the other hand, Fig. 17b presents an intriguing distribution of the shear force amplitude with three clearly marked zones. The first zone, on the left side of the figure, is distinguished by low values of A_{Fc} , while the other two zones, located on the upper and lower right side, are characterized by concentrating high values of A_{Fc} .

This implies that when the tool cutting edge is new ($V_B < 0.05$ mm), the amplitude increases proportionally to the growth of the cutting-edge radius (RPT). This trend undergoes a progressive change with the development of tool wear. In the wear interval from 0.10 to 0.17 mm, the amplitude decreases for all radii, the decrease being more pronounced at lower values of RPT . Finally, for values above $V_B = 0.17$ mm, the

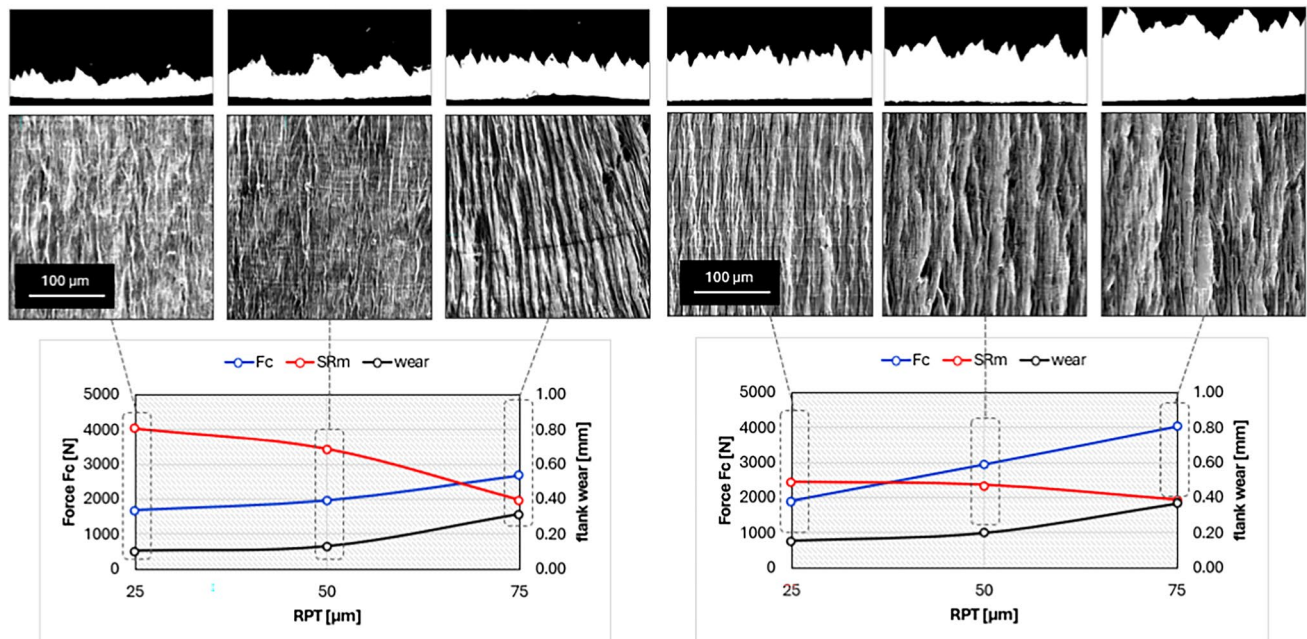


Fig. 14 Correlation between cutting force F_c versus flank wear V_B and segmentation ratio SR for cutting-edge radius of 5 μm (left) and 25 μm (right), respectively

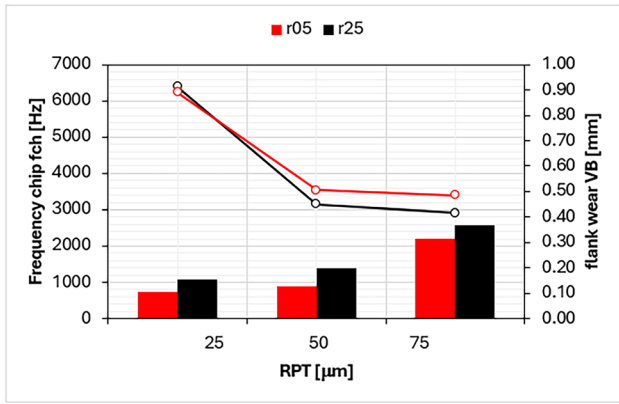


Fig. 15 Correlation between chip segmentation frequency f_{ch} versus flank wear V_B for cutting-edge radius 5 and 25 μm

amplitude resumes the increasing trend for all cutting-edge radius studied. Consequently, the combined effect of flank wear and RPT affects notably the behavior of the cutting force amplitude which could bring consequences in the cutting process. Previous research has shown that intermitencies in cutting force can induce vibrations that accelerate tool wear, negatively impacting surface integrity. This finding underscores the imperative need for a more comprehensive and in-depth study of the physico-mechanical effect associated with this behavior.

4 Conclusion

Chip formation in dry machining of Inconel 718 produced at various edge radii and rise per tooth RPT influenced by tool wear has been investigated. Based on the experimental and

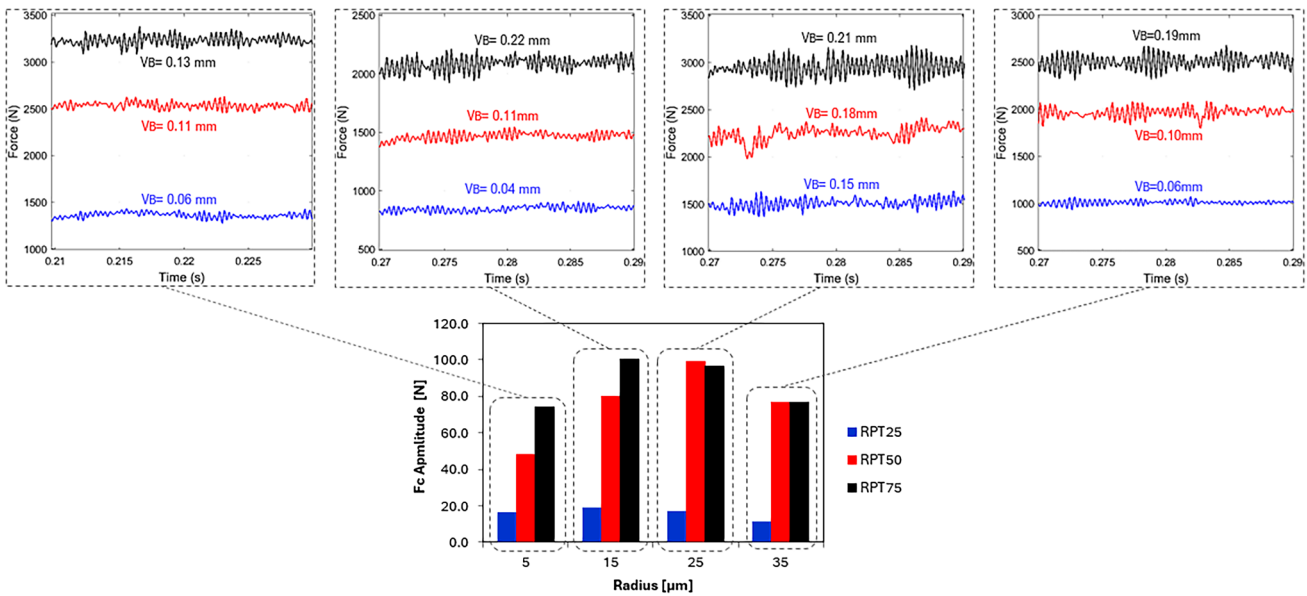
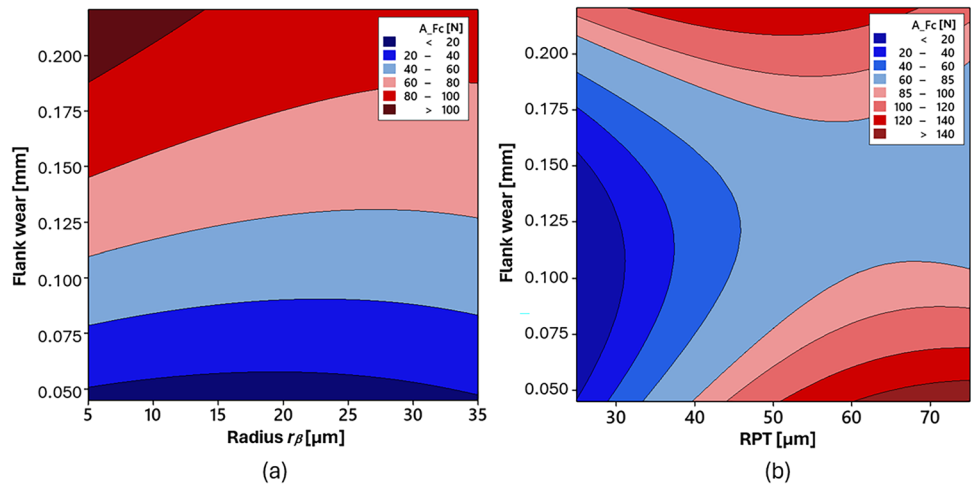


Fig. 16 Behavior of cutting amplitude A_{F_c} with changing cutting-edge radius r_β and RPT at constant cutting speed ($v_c = 20 \text{ m/min}$)

Fig. 17 Contour plot of combined effects of flank wear and cutting-edge radius r_β (a) and flank wear y RPT (b) on cutting force amplitude



numerical simulation results, the following main conclusions can be drawn:

- Chip shapes exhibit a predominantly continuous nature, but tend to transition to discontinuous types as the degree of serration increases, induced by the combination of increased flank wear with the growth of radius and *RPT*. This transition manifests itself at *SR* values below 0.5, where an *SR* of 1 indicates a continuous and complete chip.
- The compression ratio undergoes a gradual increase with increasing cutting-edge radius, indicating a higher plastic energy requirement for chip formation.
- It was observed that the width of the band (*ASB*), ranging from 1 to 2.5 μm in all cases studied, denotes a highly localized concentration of deformation in a small area, suggesting adiabatic shear failure. The results of the numerical simulations support this theory of failure.
- An 80% correlation was identified between flank wear and the increase in shear force oscillation amplitude. It is inferred that flank wear contributes to system vibration by amplifying the shear force oscillation. However, the behavior of the cutting force oscillations is diverse when combining the effect of flank wear with tool radius at different *RPT*, an aspect that requires further exploration in future studies.
- Chip morphological analysis not only provides a deeper understanding of the chip formation mechanism, but also proves to be a valuable indicator of tool wear under low-speed machining conditions, such as those employed in broaching.

Acknowledgements Cutting tools were improved with the help of “Nueva producción de herramientas orientadas para fabricar componente de alto valor añadido de turbomaquinaria” (“haute couture taylor made”), reference: PDC2021-121792-I00. Data analyses were performed with utilities developed in Project QUOLINK MCIN/AEI/501100011033/ and by the “Unión Europea NextGenerationEU/PRTR”, reference: TED2021-130044B-I00. Special thanks are addressed to company EKIN and engineer G. Celaya.

Author contribution Conceptualization: Cristian Pérez-Salinas, LN López de Lacalle. Methodology: Cristian Pérez-Salinas, Ch Sateesh Kumar. Formal analysis and investigation: Cristian Pérez-Salinas, Ander del Olmo. Writing — original draft preparation: Cristian Pérez-Salinas. Writing — review and editing: LN López de Lacalle, Ch Sateesh Kumar, Ander del Olmo. Funding acquisition: LN López de Lacalle. Resources: LN López de Lacalle. Supervision: LN López de Lacalle.

Funding Open Access funding provided thanks to the CRUE-CSIC agreement with Springer Nature. Part of the research was supported by PID2022-137380OB-I00 funded by MCIN/AEI/501100011033 and, “ERDF A way of making Europe”, by the European Union. Experimental tests were performed with support from the University Excellency groups grant by Basque Government IT 1573–22.

Declarations

Conflict of interest The authors declare no competing interests.

Open Access This article is licensed under a Creative Commons Attribution 4.0 International License, which permits use, sharing, adaptation, distribution and reproduction in any medium or format, as long as you give appropriate credit to the original author(s) and the source, provide a link to the Creative Commons licence, and indicate if changes were made. The images or other third party material in this article are included in the article’s Creative Commons licence, unless indicated otherwise in a credit line to the material. If material is not included in the article’s Creative Commons licence and your intended use is not permitted by statutory regulation or exceeds the permitted use, you will need to obtain permission directly from the copyright holder. To view a copy of this licence, visit <http://creativecommons.org/licenses/by/4.0/>.

References

1. Ezugwu EO, Wang ZM, Machado AR (1999) The machinability of nickel-based alloys: a review. *J Mater Process Technol* 86:1–16. [https://doi.org/10.1016/S0924-0136\(98\)00314-8](https://doi.org/10.1016/S0924-0136(98)00314-8)
2. Ulutan D, Ozel T (2011) Machining induced surface integrity in titanium and nickel alloys: A review. *Int J Mach Tools Manuf* 51:250–280. <https://doi.org/10.1016/j.ijmactools.2010.11.003>
3. Qi H (2012) Review of INCONEL 718 alloy: its history, properties, processing and developing substitutes. *J Mater Eng* 2:92–100
4. Aldekoa I, del Olmo A, Sastoque-Pinilla L et al (2023) Early detection of tool wear in electromechanical broaching machines by monitoring main stroke servomotors. *Mech Syst Signal Process* 204:110773. <https://doi.org/10.1016/j.ymsp.2023.110773>
5. Fernandes GHN, Barbosa LMQ, França PHP et al (2023) Towards green manufacturing: investigating tool coatings and cooling strategies for Inconel 718 turning. *The International Journal of Advanced Manufacturing Technology* 129:2257–2279. <https://doi.org/10.1007/s00170-023-12390-1>
6. Rao AS (2023) Effect of nose radius on the chip morphology, cutting force and tool wear during dry turning of Inconel 718. *Tribol – Mater, Surfaces Interfaces* 17:62–71. <https://doi.org/10.1080/17515831.2022.2160161>
7. Pérez-Ruiz JD, de Lacalle LNL, Urbikain G et al (2024) Instantaneous contact area-based model for shear strength sensitive cutting coefficients characterization of anisotropic parts. *Eng Sci Technol Int J* 52:101650. <https://doi.org/10.1016/j.jestch.2024.101650>
8. Liang X, Liu Z, Wang B (2019) State-of-the-art of surface integrity induced by tool wear effects in machining process of titanium and nickel alloys: A review. *Measurement* 132:150–181. <https://doi.org/10.1016/j.measurement.2018.09.045>
9. Mahesh K, Philip JT, Joshi SN, Kuriachen B (2021) Machinability of Inconel 718: A critical review on the impact of cutting temperatures. *Mater Manuf Processes* 36:753–791. <https://doi.org/10.1080/10426914.2020.1843671>
10. Jadam T, Datta S, Masanta M (2021) Influence of cutting tool material on machinability of Inconel 718 superalloy. *Mach Sci Technol* 25:349–397. <https://doi.org/10.1080/10910344.2020.1815047>
11. Gdula M, Mrówka-Nowotnik G (2023) Analysis of tool wear, chip and machined surface morphology in multi-axis milling process of Ni-based superalloy using the torus milling cutter.

- Wear 520–521:204652. <https://doi.org/10.1016/j.wear.2023.204652>
12. Jianhua Y, Xun L, Wenshuo Z et al (2022) A brief review on the status of machining technology of fir-tree slots on aero-engine turbine disk. *Adv Mech Eng* 14:168781322211134. <https://doi.org/10.1177/16878132221113420>
 13. del Olmo A, López de Lacalle LN, Martínez de Pissón G et al (2022) Tool wear monitoring of high-speed broaching process with carbide tools to reduce production errors. *Mech Syst Signal Process* 172:109003. <https://doi.org/10.1016/j.ymssp.2022.109003>
 14. Safran Group Fan disks for commercial turbofans. <https://www.safran-group.com/products-services/fan-disks-commercial-turbofans>. Accessed 6 Mar 2024
 15. Arrazola PJ, Rech J, M'Saoubi R, Axinte D (2020) Broaching: Cutting tools and machine tools for manufacturing high quality features in components. *CIRP Ann* 69:554–577. <https://doi.org/10.1016/j.cirp.2020.05.010>
 16. Anti A, Petrovi PB, Zeljkovi M et al (2012) The influence of tool wear on the chip-forming mechanism and tool vibrations. *Mater Technol* 46:279–285
 17. Dogra M, Sharma VS, Sachdeva A et al (2010) Tool wear, chip formation and workpiece surface issues in CBN hard turning: A review. *Int J Precis Eng Manuf* 11:341–358. <https://doi.org/10.1007/s12541-010-0040-1>
 18. Su G, Liu Z, Li L, Wang B (2015) Influences of chip serration on micro-topography of machined surface in high-speed cutting. *Int J Mach Tools Manuf* 89:202–207. <https://doi.org/10.1016/j.ijmactools.2014.10.012>
 19. Ozcatalbas Y (2003) Chip and built-up edge formation in the machining of in situ Al4C3–Al composite. *Mater Des* 24:215–221. [https://doi.org/10.1016/S0261-3069\(02\)00146-2](https://doi.org/10.1016/S0261-3069(02)00146-2)
 20. Komanduri R, Schroeder TA (1986) On Shear Instability in Machining a Nickel-Iron Base Superalloy. *J Eng Ind* 108:93–100. <https://doi.org/10.1115/1.3187056>
 21. Liu C, Wan M, Zhang W, Yang Y (2021) Chip formation mechanism of Inconel 718: A review of models and approaches. *Chin J Mech Eng* 34:34. <https://doi.org/10.1186/s10033-021-00552-9>
 22. Ye GG, Chen Y, Xue SF, Dai LH (2014) Critical cutting speed for onset of serrated chip flow in high speed machining. *Int J Mach Tools Manuf* 86:18–33. <https://doi.org/10.1016/j.ijmactools.2014.06.006>
 23. Chandra Behera B, Sudarsan Ghosh C, Paruchuri VR (2019) Study of saw-tooth chip in machining of Inconel 718 by metallographic technique. *Mach Sci Technol* 23:431–454. <https://doi.org/10.1080/10910344.2019.1575397>
 24. Cui X, Zhao B, Jiao F, Zheng J (2016) Chip formation and its effects on cutting force, tool temperature, tool stress, and cutting edge wear in high- and ultra-high-speed milling. *Int J Adv Manuf Technol* 83:55–65. <https://doi.org/10.1007/s00170-015-7539-7>
 25. Ross NS, Sheeba PT, Shibi CS et al (2024) A novel approach of tool condition monitoring in sustainable machining of Ni alloy with transfer learning models. *J Intell Manuf* 35:757–775. <https://doi.org/10.1007/s10845-023-02074-8>
 26. Li X, Shi JJ, Cao GH et al (2019) Improved plasticity of Inconel 718 superalloy fabricated by selective laser melting through a novel heat treatment process. *Mater Des* 180:107915. <https://doi.org/10.1016/j.matdes.2019.107915>
 27. Moiz M (2013) The influence of grain size on the mechanical properties of Inconel 718. Linköping University, Engineering Materials
 28. Singh SR, Mote RG, Mishra SK (2022) The effect of microstructures and precipitates (γ' , γ'' , δ) on machinability of Inconel-718 nickel-based superalloy in turning process. *J Manuf Process* 82:374–389. <https://doi.org/10.1016/j.jmapro.2022.08.004>
 29. Arunachalam R, Mannan MA (2000) Machinability of Nickel-based high temperature alloys. *Mach Sci Technol* 4:127–168. <https://doi.org/10.1080/10940340008945703>
 30. AMS-5662 (2022) Aerospace Material Specification 5662L, Nickel Alloy Corrosion and Heat Resistant Bars, Forgings and Rings. SAE International. <https://www.sae.org/standards/content/ams5662/>. Accessed 02 May 2024
 31. Special Metals (2007) INCONEL® alloy 718. <https://www.specialmetals.com/documents/technical-bulletins/inconel/inconel-alloy-718.pdf>. Accessed 02 May 2024
 32. Komanduri R, Brown RH (1981) On the mechanics of chip segmentation in machining. *J Eng Ind* 103:33–51. <https://doi.org/10.1115/1.3184458>
 33. Bayoumi AE, Xie JQ (1995) Some metallurgical aspects of chip formation in cutting Ti-6wt.%Al-4wt.%V alloy. *Mater Sci Eng, A* 190:173–180. [https://doi.org/10.1016/0921-5093\(94\)09595-N](https://doi.org/10.1016/0921-5093(94)09595-N)
 34. Parida AK (2019) Analysis of Chip Geometry in Hot Machining of Inconel 718 Alloy. *Iran J Sci Technol Trans Mech Eng* 43:155–164. <https://doi.org/10.1007/s40997-018-0146-0>
 35. Halim NHA, Haron CHC, Ghani JA, Azhar MF (2019) Tool wear and chip morphology in high-speed milling of hardened Inconel 718 under dry and cryogenic CO₂ conditions. *Wear* 426–427:1683–1690. <https://doi.org/10.1016/j.wear.2019.01.095>
 36. Airao J, Khanna N, Nirala CK (2022) Tool wear reduction in machining Inconel 718 by using novel sustainable cryo-lubrication techniques. *Tribol Int* 175:107813. <https://doi.org/10.1016/j.triboint.2022.107813>
 37. Sowerby R, Chandrasekaran N (1989) A proposal for the onset of chip segmentation in machining. *Mater Sci Eng, A* 119:219–229. [https://doi.org/10.1016/0921-5093\(89\)90541-8](https://doi.org/10.1016/0921-5093(89)90541-8)
 38. Kouadri S, Necib K, Atlati S et al (2013) Quantification of the chip segmentation in metal machining: Application to machining the aeronautical aluminium alloy AA2024-T351 with cemented carbide tools WC-Co. *Int J Mach Tools Manuf* 64:102–113. <https://doi.org/10.1016/j.ijmactools.2012.08.006>
 39. Atlati S, Haddag B, Nouari M, Zenasni M (2011) Analysis of a new Segmentation Intensity Ratio “SIR” to characterize the chip segmentation process in machining ductile metals. *Int J Mach Tools Manuf* 51:687–700. <https://doi.org/10.1016/j.ijmactools.2011.05.007>
 40. Duan CZ, Wang MJ, Pang JZ, Li GH (2006) A calculational model of shear strain and strain rate within shear band in a serrated chip formed during high speed machining. *J Mater Process Technol* 178:274–277. <https://doi.org/10.1016/j.jmatprotec.2006.04.008>
 41. Davis B, Dabrow D, Newell R et al (2018) Chip morphology and chip formation mechanisms during machining of ecae-processed titanium. *J Manuf Sci Eng* 140. <https://doi.org/10.1115/1.4038442>
 42. Johnson GR (1983) A constitutive model and data for metals subject to large strains, high strain rate and high temperatures. In: *Proc. of 7th Int. Symp. on Ballistics*, The Hague: Neth 541–547
 43. Calamaz M, Coupard D, Girod F (2008) A new material model for 2D numerical simulation of serrated chip formation when machining titanium alloy Ti–6Al–4V. *Int J Mach Tools Manuf* 48:275–288. <https://doi.org/10.1016/j.ijmactools.2007.10.014>
 44. Jafarian F, Imaz Ciaran M, Umbrello D et al (2014) Finite element simulation of machining Inconel 718 alloy including microstructure changes. *Int J Mech Sci* 88:110–121. <https://doi.org/10.1016/j.ijmecsci.2014.08.007>
 45. Klocke F, Lung D, Buchkremer S (2013) Inverse Identification of the Constitutive Equation of Inconel 718 and AISI 1045 from FE Machining Simulations. *Procedia CIRP* 8:212–217. <https://doi.org/10.1016/j.procir.2013.06.091>
 46. Fabián Pérez-Salinas C, Fernández-Lucio P, del Olmo A et al (2023) The influence of cutting edge microgeometry on the

- broaching of Inconel 718 slots. *Eng Sci Technol Int J* 48:101563. <https://doi.org/10.1016/j.jestch.2023.101563>
47. Arrazola PJ, Özel T, Umbrello D et al (2013) Recent advances in modelling of metal machining processes. *CIRP Ann* 62:695–718. <https://doi.org/10.1016/j.cirp.2013.05.006>
 48. Sun S, Brandt M, Dargusch MS (2017) Effect of tool wear on chip formation during dry machining of Ti-6Al-4V alloy, part 1: Effect of gradual tool wear evolution. *Proc Inst Mech Eng B J Eng Manuf* 231:1559–1574. <https://doi.org/10.1177/0954405415599956>
 49. Black JT (1972) Shear front-lamella structure in large strain plastic deformation processes. *J Eng Ind* 94:307–313. <https://doi.org/10.1115/1.3428132>
 50. Belhadi S, Mabrouki T, Rigal J-F, Boulanouar L (2005) Experimental and numerical study of chip formation during straight turning of hardened AISI 4340 steel. *Proc Inst Mech Eng B J Eng Manuf* 219:515–524. <https://doi.org/10.1243/095440505X32445>
 51. Sun S, Brandt M, Dargusch MS (2009) Characteristics of cutting forces and chip formation in machining of titanium alloys. *Int J Mach Tools Manuf* 49:561–568. <https://doi.org/10.1016/j.ijmactools.2009.02.008>
 52. Rowe RA, Allison PG, Palazotto AN, Davami K (2022) Adiabatic shear banding in nickel and nickel-based superalloys: a review. *Metals (Basel)* 12:1879. <https://doi.org/10.3390/met12111879>
 53. Pawade RS, Joshi SS (2011) Mechanism of chip formation in high-speed turning of Inconel 718. *Mach Sci Technol* 15:132–152. <https://doi.org/10.1080/10910344.2011.557974>
 54. Joshi S, Tewari A, Joshi SS (2015) Microstructural characterization of chip segmentation under different machining environments in orthogonal machining of Ti6Al4V. *J Eng Mater Technol* 137. <https://doi.org/10.1115/1.4028841>
 55. la Monaca A, Axinte DA, Liao Z et al (2022) Temperature-dependent shear localisation and microstructural evolution in machining of nickel-base superalloys. *Mater Des* 219:110792. <https://doi.org/10.1016/j.matdes.2022.110792>
 56. Clos R, Schreppel U, Veit P (2003) Temperature, microstructure and mechanical response during shear-band formation in different metallic materials. *J Phys IV (Proceedings)* 110:111–116. <https://doi.org/10.1051/jp4:20020679>
 57. Hao Z, Cui R, Fan Y (2018) Formation mechanism and characterization of shear band in high-speed cutting Inconel718. *Int J Adv Manuf Techno* 98:2791–2799. <https://doi.org/10.1007/s00170-018-2435-6>
 58. Yaich M, Ayed Y, Bouaziz Z, Germain G (2017) Numerical analysis of constitutive coefficients effects on FE simulation of the 2D orthogonal cutting process: application to the Ti6Al4V. *Int J Adv Manuf Technol* 93:283–303. <https://doi.org/10.1007/s00170-016-8934-4>
 59. Song X, He W, Ihara T (2023) A novel approach for dry cutting inconel 718 in a more sustainable and low-cost way by actively and purposely utilizing the built-up layer. *Micromachines (Basel)* 14:1787. <https://doi.org/10.3390/mi14091787>
 60. Grzesik W, Niesłony P, Habrat W et al (2018) Investigation of tool wear in the turning of Inconel 718 superalloy in terms of process performance and productivity enhancement. *Tribol Int* 118:337–346. <https://doi.org/10.1016/J.TRIBOINT.2017.10.005>
 61. Song XQ, Takahashi Y, He WM, Ihara T (2017) On the formation mechanisms of adhering layer during machining metal material. *Key Eng Mater* 749:39–45. <https://doi.org/10.4028/www.scientific.net/KEM.749.39>
 62. Petrovic PB, Zeljković M, Kosec B et al (2012) The influence of tool wear on the chip-forming mechanism and tool vibrations. *Materiali in tehnologije* 279–285

Publisher's Note Springer Nature remains neutral with regard to jurisdictional claims in published maps and institutional affiliations.